Chapter 6

The Effect of Aluminium Impurities on Collision Cascades in MgO

Much of this work has previously been published in Nuclear Instruments and Methods in Physics Research Section B: Beam Interactions with Materials and Atoms [4]

6.1 Introduction

Whilst recent molecular dynamics studies on metals have examined the interaction of cascade events in alloys (i.e. disordered combinations of metals) and near defects like grain boundaries [271–273], no previous work on ceramic

systems has taken account of deviations from perfect systems free from any kind of defect (examples of work on pure systems include [264,265,274–276]). The idea that a conventional ceramic such as MgO is free from defects is, of course, a fallacy. The influence of even a small concentration of impurities on the evolution of a damage cascade has, however, never been considered. This is, perhaps, understandable since a realistic level of impurity is tenths of a percent. In this study, 0.2% of the Mg^{2+} cations will be replaced with Al^{3+} ions (i.e. substitutionally). This will cause a charge imbalance which needs to be compensated. Previous work has shown that by far the lowest energy charge compensation mechanism is facilitated by Mg^{2+} vacancies [277]. Thus 0.1% of the original Mg^{2+} ions are removed to leave vacant lattice sites. Overall this is equivalent to doping MgO with Al_2O_3 as in equation 6.1.

$$Al_2O_3 + 3Mg_{Mg}^{\times} + 3O_O^{\times} \rightarrow 2Al_{Mg}^{\bullet} + V_{Mg}^{''} + 3MgO \tag{6.1}$$

Although 0.2% Al^{3+} ions and 0.1% cation vacancies is a small concentration of defects, there are strong Coulomb interactions between the species. Consequently neutral defect clusters will form of the type $\left\{Al_{Mg}^{\bullet} : V_{Mg}^{''} : Al_{Mg}^{\bullet}\right\}^{\times}$. The structure of such defect clusters has been investigated previously and shown to be linear such that the three defects are aligned along <100> [277]. The change in lattice parameter with defect concentration predicted from such a defect cluster model has been shown to afford good agreement with experimental observations. Thus, the simulation cell will consist of an otherwise perfect MgO lattice with these defect clusters randomly distributed in order to reach this concentration of impurities. An example of the cell used is given later on in the methodology section (Section 6.3).

The aim of this study is to analyse the effect of impurities in ceramics on cascade events specifically for the ceramic MgO. This was chosen for the same reason as in the electron irradiation study by Kinoshita *et al.* [278], that is it is a simple model material that can give insights into general effects without the complexities that other multicomponent cation solids might present.

Here, PKAs of 1 keV and 2 keV will be modelled using atomic scale molecular dynamics simulation (MD). A set of twenty distinct directions have been selected and both Mg^{2+} and O^{2-} PKAs will be modelled in each case. The crucial difference between this study and previous research is that here both atomically pure and aluminium doped systems are considered. Thus a total of 40 simulations are carried out within a pure MgO lattice and a further 40 simulations for a doped MgO lattice (for the same set of directions, which start from different points within the simulation cell).

6.2 Literature Review

6.2.1 Background

Kinchin and Pease (K-P) first reported a model to describe the accumulation of radiation induced damage exactly fifty years ago [279]. Since this time a number of approximations and limitations of the model have been discussed and improvements suggested (see for example [280–284]). Nevertheless, K-P (albeit modified) is still widely used as a basis for the discussion of results generated experimentally and via computer modelling. Indeed K-P was re-

cently used to discuss atomic scale computer simulation results of cascade damage in MgO [285]. Fifty years ago computer simulation did not even exist!

The K-P model provides an estimation of the number of atoms permanently displaced from their lattice sites (N_d) per primary knock-on atom (PKA) by means of the relations shown in Table 6.1, where E is the energy of the PKA and E_d is the threshold energy.

N_d	Energy (E) of PKA
0	$0 < E < E_d$
1	$E_d < E < 2E_d$
$\frac{E}{2E_d}$	$2E_d < E < E_1$
$\frac{E_1}{2E_d}$	$E_1 < E < ?$

Table 6.1: The Kinchin - Pease (K-P) model criteria [279–282]

Inherent in the model is the assumption that recoil atoms lose energy in excess of E_1 only through electron excitation. Below E_1 the recoil atoms lose energy only through hard-core elastic scattering. Furthermore, if an atom receives energy greater than E_d, it is permanently displaced and if an atom receives energy less than E_d, it will return to its lattice site. This applies to any atom in the lattice being displaced as a consequence of a PKA incident from any direction. Consequently since K-P does not account for recombination, it predicts a maximum number of displaced atoms which will become important when it comes to the analysis of the results.

Amongst the most prominent deficiencies of this most simple interpretation of K-P is therefore the lack of crystal species differentiation. In a ceramic material such as MgO, there are two differently charged species of usually

quite different sizes. It seems unlikely that they will exhibit the same displacement energies (and, in fact, in MgO they do not [285]). This could be corrected simply by having two values of E_d, one for the cation and one for the anion [284]. However, this does not correct for the crystallographic anisotropy associated with the PKA incident direction. Numerous modelling studies have shown that, for a range of materials, E_d (or N_d) can vary considerably with incident direction (see for example [119, 285–287]). A single value of E_d within K-P therefore represents some sort of average over both species and crystallographic direction. All of these studies were performed on atomistically pure systems and it seems likely that a random distribution of aliovalent defects would tend to disrupt this and make the system behave more isotropically.

6.2.2 MgO

MgO is an engineering ceramic with a huge range of uses from buffer layers to produce highly textured superconducting films exploiting the lattice parameter [288] to electrical insulation in heating elements which require moderate thermal conductivities and a high electrical resistivity [289]. Due to this huge range of uses it is one of the most well understood materials and this, combined with the fact that it has also been successfully modelled using pair potentials [277, 286, 290–293] makes it logical for this simple material to be used in this first study of the effect impurities have on collision cascades.

Crystallography

MgO is one of the most simple oxides and forms in the rock-salt crystal structure with a lattice parameter of 4.214 Å [294]. It consists of close packed oxygen ions with all of the octahedral interstitial positions occupied by magnesium ions. This is show in figure 6.1.

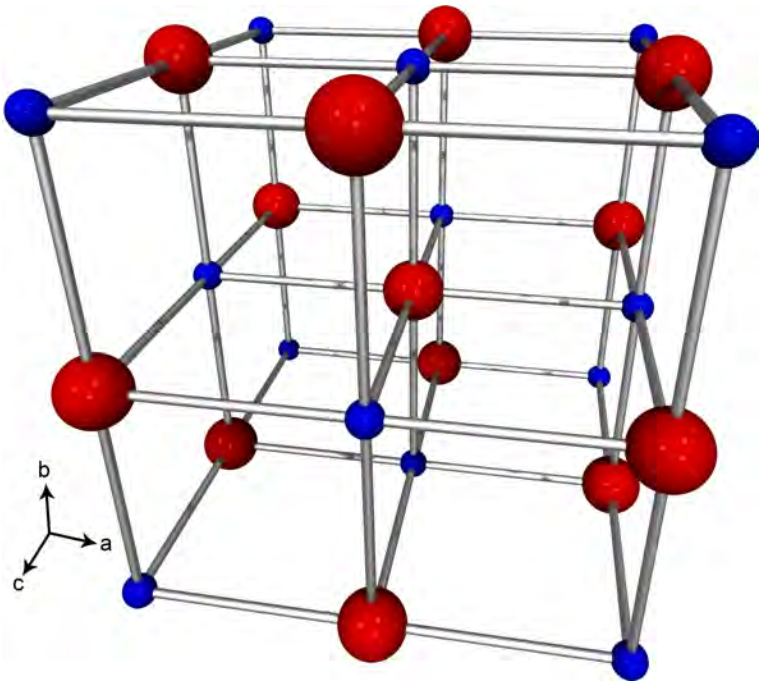

Figure 6.1: A full unit cell of MgO (generated using structural data from [294]). Smaller blue spheres are Mg^{2+} ions and larger red spheres represent O^{2-} ions.

6.2.3 Previous Studies in MgO

Kinoshita *et al.* [278] examined the kinetics of point defects formed by the electron irradiation of MgO in the mid 1980s. They irradiated single crystals of MgO from different sources with 1 MeV electrons at a range of tempera-

tures between 25 °C and 1000 °C [278]. They found that at low temperatures of about 330 °C, interstitial dislocation loops tend to nucleate but that as the irradiation temperature is increased, the density of these loops tends to decrease and they take on an obvious loop shape see figures 6.2 and 6.3 (these are figures 2 and 4 from Kinoshita *et al.* [278]) which show the low and high temperature irradiations respectively. By considering the kinetics of the system [278] (which is beyond the scope of this study) they concluded that interstitial loops nucleate from one or two pairs of Mg and O interstitials below 600 °C and that growth of these loops occurs above 600 °C.

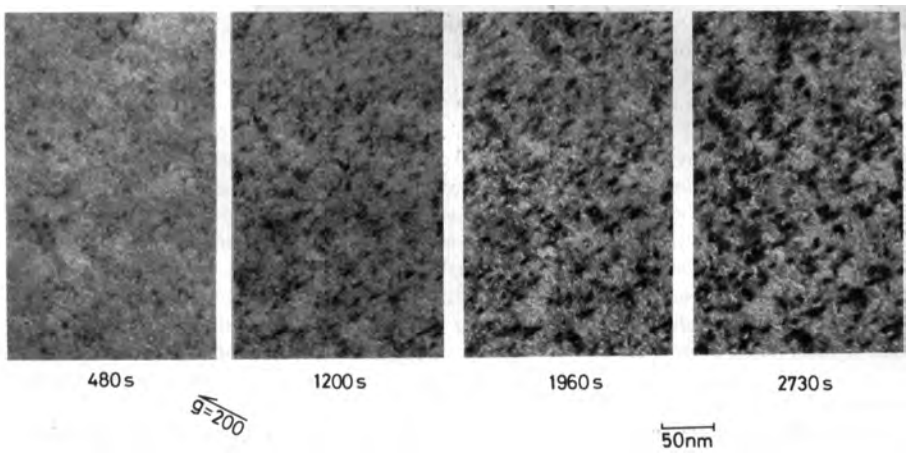

Figure 6.2: Formation and growth of interstitial dislocation loops in MgO irradiated aproximately along <001> at 600 K with a 1 MeV electron flux of 2×10^{23} e/m^2 (reproduced from [278]).

Alves *et al.* recently carried out some work into the recovery from radiation damage in MgO for both pure samples and samples doped with 400 ppm Li doped MgO [295]. In this work, they irradiated single crystals of pure and Li doped MgO with 175 keV Li^+ ions to a dose of 1×10^{17} ions/cm^2 and analysed the damage and recovery at various temperatures using Rutherford Backscattering/Channelling Spectroscopy(RBS) and optical absorption spec-

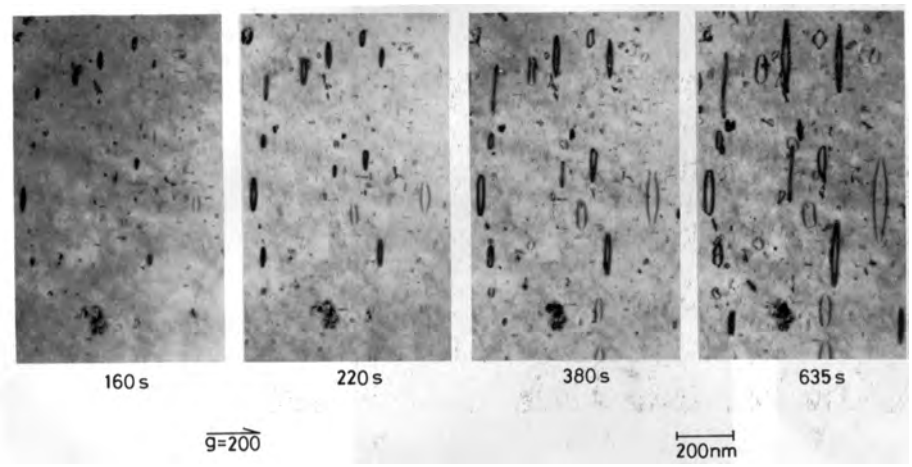

Figure 6.3: Formation and growth of interstitial dislocation loops in MgO irradiated aproximately along <001> at 1085 K with a 1 MeV electron flux of 4×10^{23} e/m^2. The loops are perfect dislocation loops with $\frac{1}{2}$<101> Burgers vectors lying on (101) planes elongated along <010> directions (reproduced from [278]).

troscopy. They found that for both pure and doped samples, implantation of Li^+ ions causes significant damage as shown by the enhanced dechannelling in the RBS measurements [295]. Alves *et al.* found that for the Li doped sample, after annealing at 1250 K the damage responsible for the dechannelling had virtually completely disappeared. The pure case was more complicated due to polishing damage on the surface causing dechannelling to a depth of 200nm [295]. They noted implantation damage below this depth due to the implantation of Li. Upon annealing at temperatures of 1025K they found the dechannelling yield in the deeper region fell off from an initial 70% to 48% [295]. They do not report a similar state for the doped sample or a result for annealing at 1250 K for the pure sample, making comparison difficult. They do, however, report an intermediate annealing temperature of 875 K for the pure sample where the normalised dechannelling yield is 56%. This

may be indicative that doping with Li increases the ability for the material to recover from radiation damage.

Considering next the optical absorption results. Before implantation, the Li doped sample showed a strong absorption band at 1.8 eV which Alves *et al.* associated with the $[Li]^0$ centres. After implantation this was joined by another strong absorption peak at 5.0 eV which they associated with F^+ centres (an electron trapped at an anion vacancy) [295]. Upon annealing the damage causing the 5.0 eV peak was eliminated and this also causes the intensity of the 1.8 eV band ($[Li]^0$ to decrease [295]. Alves *et al.* [295] found that recovery of defects in the damaged pure sample starts at about 500 K and recovery was complete at 1250 K.

Gonzáles *et al.* [296] also looked at Li doped MgO but they examined its properties under neutron irradiation at energies greater than 100 KeV. Again single crystals of MgO were used and pure and doped samples were irradiated. Two dopants were considered. The first set, as in the previous study, was doped with 400 ppm Li ions and the other set was doped with an undocumented concentration of hydrogen [296]. All three groups were irradiated at temperatures of 325 $\pm$ 20 K. Analysis of the damage was performed using optical absorption spectroscopy. Gonzáles *et al.* found (as Alves *et al.* confirm [295]) that irradiation of MgO produces F^+ centres in the MgO causing a large absorption band at 5.0 eV. In [296] they show a log-log plot of neutron dose against the absorption coefficient of the 5 eV band (and link this directly to the concentration of F^+ centres) and they find that below 1×10^{18} neutrons per cm^2 (above which all samples are virtually identical) the pure case

shows the highest concentration, followed by the hydrogen doped case and finally the least damaged sample is the Li doped MgO [296]. They compare this result with previous work by Sibley and Chen [297] which appears to show conflicting results. Sibley and Chen [297] noted that a sample containing 50 ppm Fe ions showed the opposite effect, i.e. it damaged faster than the pure case and they attributed this to the trapping of displaced interstitials by impurities thus preventing them from recombining with vacancies [297].

By doping with hydrogen Gonzáles *et al.* created a very cloudy crystal containing high concentrations of cavities about 0.6 μm in size containing hydrogen gas [296]. They found that after irradiation to 1×10^{17} neutrons/cm^2 the size of the 5.0 eV peak associated with anion vacancies and F^+ centres is obviously smaller corresponding to a 35% lower vacancy concentration [296]. They attribute this decrease in anion vacancy concentration to the migration of these vacancies to the hydrogen filled cavities, an effect proposed by originally Henderson *et al.* [298]. After the same neutron dose, the Li doped sample showed an even lower anion vacancy concentration than the hydrogen doped sample with 70% fewer than the pure case although as mentioned earlier, this suppression of vacancy formation disappears at higher doses of 1×10^{18} n/cm^2. Gonzáles *et al.* propose that the reason for the reduced vacancy concentration is partly due to the presence of hydrogen filled microcavities that have been previously observed in Li doped MgO [296] although they state that this can only account for a small amount of the total. They go on to state that the main reason for the apparent loss of oxygen vacancies is due to the capture of hydride ions, thus causing them to be camouflaged as $[H^-]^+$ centres (an oxygen vacancy occupied by a proton).

The conflicting results obviously require further work to clarify exactly what occurs.

These studies on nominally pure and intentionally doped samples show that even in a very simple ceramic system very complex damage and recovery processes occur. The use of atomistic simulation can help in the understanding of such complicated systems by eliminating some of the unknowns. While it is not possible (or at least very difficult) to examine a single cascade in a real material, it is possible to carry out many simulations and construct an average cascade. Efforts should be made to examine carefully the behaviour of defects indicated in the experimental work. Unfortunately it is very difficult to model F^+ centres with MD simulations as these are electronic defects. As such a full electronic structure model may be required to simulate them correctly. Others, such as the hydrogen ion trapped on an anion vacancy are much easier to simulate and if MD simulations are performed it should be simple to test whether this defect forms. Other simulations could be performed to measure activation energies for the diffusion of anion vacancies to surfaces although, this seems somewhat unlikely as it has been shown that interstitial migration barriers are much lower than those for vacancies in MgO [299].

6.3 Methodology

The potentials that describe the interactions between ions were derived previously to model cascades in $MgAl_2O_4$ spinel [119]. They assume full ionic

charges on all ions with the Coulomb interactions calculated using the fast multipole method implemented by Rankin [120]. Additional pairwise additive short-range interactions of the Buckingham form also operate between ions [119] and these parameters are listed in table 6.2. A smooth cutoff is applied to these terms at distances greater than 7.4 Å for anion - anion interactions and 5.0 Å for cation - anion interactions. At the very short inter-ionic distances experienced by particles in the initial phase of the cascade, the potential was replaced by a screened Coulomb interaction [300]. This was smoothly splined to the outer potential by ensuring that the first and second derivatives were continuous.

Table 6.2: Full charge short range potential parameters used to describe interactions between all the ions in this study. Reproduced from [4].

Species	A (eV)	ρ (eV)	C (eV Å^6)
$O^{2-} \leftrightarrow O^{2-}$	9547.960	0.21916	32.00
$Mg^{2+} \leftrightarrow O^{2-}$	1279.69	0.29969	0.00
$Al^{3+} \leftrightarrow O^{2-}$	1374.79	0.30130	0.00

The molecular dynamics simulations were carried out in charge neutral simulation cells that contained either 48669 Mg^{2+} cations, and 48669 O^{2-} anions in the pure lattice cases or 48522 Mg^{2+}, 98 Al^{3+} cations and 48669 O^{2-} anions for the doped lattice simulations. The velocity Verlet algorithm was used to evolve the system as implemented in the code LBOMD [125] and described in chapter 3. The cell was simulated using non-periodic boundary conditions with the outer 2 layers of atoms fixed. An image showing the distribution of the defects in the cell is shown in figure 6.4.

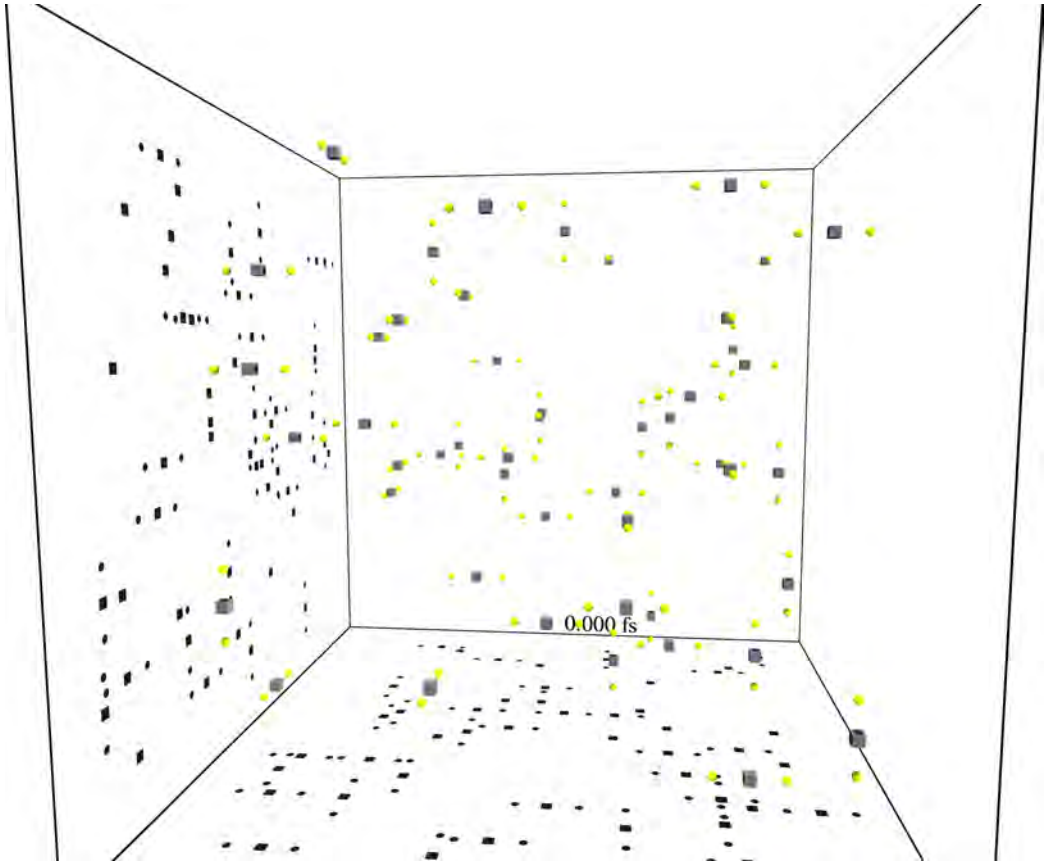

Figure 6.4: Starting configuration for all cascades doped with 0.2% Al. Grey cubes represent V''_{Mg} and yellow spheres represent $Mg^{\bullet}_{Al}$. Shadows are projected onto both the left and bottom faces in order to aid three dimensional visualisation.

6.4 Results and Discussion

Before the results of the radiation damage cascade simulations are discussed the simulated properties of MgO will be compared with experimental (e) and *ab inito* simulation values (s). These results are shown in table 6.3. As can be seen the potentials reproduce the structure very well with the lattice parameter within 0.36% of experimental values.

Table 6.3: Comparison of the predicted lattice parameter with experimental and *ab initio* simulation data

Source	Lattice Parameter (Å)	% Difference
Predicted	4.199	N\A
Tsirel'son *et al.* [294] (e)	4.214	0.36
McCarthy and Harrison [301] (s)	4.195	-0.10
Taylor [302] (e)	4.211	0.29
Hirata *et al.* [303] (e)	4.203	0.10

6.4.1 Variation with Direction and Doping

In order to quantify the effect that a displacement cascade has on the lattice it is necessary to select a number of criteria by which the damage process can be assessed. This can include, for example, properties such as the peak number of Frenkel pairs (P_F) and the time at which this occurred (P_t). These are measures of the damage progression and occur towards the end of the ballistic stage of the cascade (≈0.1 ps). Other properties include the total number (N_d) and types of residual defects left once the thermal-spike has dissipated (≈6 ps). At this point the ions in the damaged region are close to being in thermal equilibrium with the remainder of the lattice. There can, however, be considerable energy retained by those residual defects. Related to this is the final number of atoms (N_T) displaced from their original lattice sites (even if they return to equivalent lattice sites) since it provides an alternative measure of how much the lattice has been disrupted and is the equivalent of N_d in K-P. Finally, the maximum distance between residual defects is reported. This is a particularly simple way to estimate the effective size of the cascade (more sophisticated measures based on volume are under development).

Results for these six criteria are presented in Table 6.4a and 6.4b for 1 keV PKA cascades and in Table 6.5a and 6.5b for 2 keV PKA cascades. For each table the first set of columns report results for the undoped (pure) lattice, the middle set of columns are for the alumina doped lattice and the third set show differences between doped and pure results. Beneath each column is the property value average over all directions. Under the average is the standard deviation (SD) in the property value.

The first point to recognise is that the property values for the undoped cases show considerable variation with PKA incident direction, in agreement with previous observations [119, 285–287]. Nevertheless, all the average property values are large compared to their SDs. In general terms, for the alumina doped lattice simulations, the situation is very similar: considerable variation in property values between directions is observed. Furthermore, the average values generated in the doped lattice are not so different to those for the undoped lattice (within a SD). However, for a specific direction, and for a specific PKA type and energy, the results for the undoped and doped lattice simulations are often considerably different (simply follow across rows in Tables 6.4 and 6.5). This is made clear by the variation of values in the third set of difference columns. The average differences for a given property are also calculated. These average difference values are always smaller than the corresponding standard deviations and in some cases dramatically so. Conversely and crucially the average difference values are small compared to the absolute property values.

The dopant level investigated here, 0.2% Mg^{2+} replaced by Al^{3+}, is clearly

a)

	Pure									Doped									Difference								
Direction	Peak No Frenkel Pairs (P_F)	Peak Time (fs) (P_T)	Displaced Atoms (N_T)	Total Defects (N_d)	Total Mg_i	Total O_i	Total V_{Mg}	Total V_O	Max dist between defects (Å)	Peak No Frenkel Pairs (P_F)	Peak Time (P_T) (fs)	Displaced Atoms (N_T)	Total Defects (N_D)	Total Mg_i	Total O_i	Total V_{Mg}	Total V_O	Max dist between defects (Å)	Peak No Frenkel Pairs (P_F)	Peak Time (fs) (P_T)	Displaced Atoms (N_T)	Total Defects (N_d)	Total Mg_i	Total O_i	Total V_{Mg}	Total V_O	Max dist between defects (Å)
021	87	86.7	23	8	2	2	2	2	36.4	124	97.2	23	10	3	2	3	2	13.6	37	10.6	0	2	1	0	1	0	-22.7
100	73	88.1	17	6	2	1	2	1	18.0	114	96.8	22	10	2	2	4	2	21.5	41	8.7	5	4	0	1	2	1	3.5
10 31	72	128.6	22	8	3	1	3	1	33.4	99	109.7	26	8	2	2	2	2	25.9	27	-18.9	4	0	-1	1	-1	1	-7.5
10 52	71	94.7	10	6	2	1	2	1	33.4	86	101.2	33	12	2	4	2	4	53.9	15	6.4	23	6	0	3	0	3	20.5
110	77	85.4	19	6	2	1	2	1	29.4	98	99.2	22	6	2	1	3	1	26.6	21	13.8	3	0	0	0	1	0	-2.8
111	102	97.0	22	6	1	2	1	2	29.2	83	90.1	19	8	3	1	3	1	23.1	-19	-7.0	-3	2	2	-1	2	-1	-6.1
123	84	98.9	13	6	2	1	2	1	27.8	113	89.1	22	2	1	0	1	0	20.6	29	-9.8	9	-4	-1	-1	-1	-1	-7.2
134	101	88.3	24	10	3	2	3	2	22.4	80	93.0	30	9	1	3	2	3	32.8	-21	4.7	6	-1	-2	1	-1	1	10.4
221	101	103.1	23	8	3	1	3	1	32.7	79	91.0	15	4	0	1	2	1	25.6	-22	-12.1	-8	-4	-3	0	-1	0	-7.2
257	85	95.7	24	2	1	0	1	0	26.0	89	99.8	29	4	0	1	2	1	17.8	4	4.2	5	2	-1	1	1	1	-8.2
432	96	108.7	14	2	1	0	1	0	35.8	94	97.7	19	8	2	2	2	2	27.5	-2	-11.1	5	6	1	2	1	2	-8.2
522	81	95.4	18	8	3	1	3	1	26.7	124	84.1	22	7	2	1	3	1	23.4	43	-11.3	4	-1	-1	0	0	0	-3.3
537	86	96.6	15	8	3	1	3	1	33.5	73	104.6	13	2	1	0	1	0	40.6	-13	8.0	-2	-6	-2	-1	-2	-1	7.1
20 74	91	103.6	20	6	2	1	2	1	34.4	100	90.4	21	5	1	1	3	1	16.5	9	-13.2	1	-1	-1	0	1	0	-17.8
441	58	105.2	17	10	4	1	4	1	34.5	105	113.0	10	4	2	0	2	0	28.8	47	7.8	-7	-6	-2	-1	-2	-1	-5.7
443	99	91.1	16	6	1	2	1	2	32.7	127	114.2	21	5	1	1	2	1	16.9	28	23.1	5	-1	0	-1	1	-1	-15.9
510	82	88.2	17	6	2	1	2	1	31.8	81	84.7	25	6	1	2	2	2	25.7	-1	-3.5	8	0	-1	1	0	1	-6.1
511	73	99.7	18	4	1	1	1	1	32.8	110	100.9	17	4	1	1	2	1	29.0	37	1.2	-1	0	0	0	1	0	-3.8
533	96	93.4	25	6	2	1	2	1	21.5	103	102.9	27	9	1	3	2	3	21.4	7	9.4	2	3	-1	2	0	2	-0.1
860	122	98.2	27	8	2	2	2	2	23.2	110	91.4	15	7	2	1	2	1	24.6	-12	-6.9	-12	-1	0	-1	0	-1	1.4
Average	86.85	97.33	19.20	6.50	2.10	1.15	2.10	1.15	29.79	99.60	97.55	21.55	6.50	1.50	1.45	2.25	1.45	25.80	12.75	0.21	2.35	0.00	-0.60	0.30	0.15	0.30	-3.99
SD	14.60	9.81	4.48	2.14	0.85	0.59	0.85	0.59	5.26	16.31	8.58	5.84	2.76	0.83	1.05	0.72	1.05	8.99	22.94	11.10	7.31	3.39	1.19	1.17	1.18	1.17	9.72

b)

	Pure									Doped									Difference								
Direction	Peak No Frenkel Pairs (P_F)	Peak Time (fs) (P_T)	Displaced Atoms (N_T)	Total Defects (N_d)	Total Mg_i	Total O_i	Total V_{Mg}	Total V_O	Max dist between defects (Å)	Peak No Frenkel Pairs (P_F)	Peak Time (fs) (P_T)	Displaced Atoms (N_T)	Total Defects (N_d)	Total Mg_i	Total O_i	Total V_{Mg}	Total V_O	Max dist between defects (Å)	Peak No Frenkel Pairs (P_F)	Peak Time (fs) (P_T)	Displaced Atoms (N_T)	Total Defects (N_d)	Total Mgi	Total Oi	Total VMg	Total VO	Max dist between defects (Å)
021	93	91.9	16	6	0	3	0	3	23.0	92	92.9	15	2	0	1	0	1	21.7	-1	1.0	-1	-4	0	-2	0	-2	-1.3
100	70	83.8	9	6	2	1	2	1	23.6	77	88.7	12	4	0	1	2	1	22.2	7	4.9	3	-2	-2	0	0	0	-1.3
10 31	79	91.4	22	8	2	2	2	2	40.5	75	91.3	10	4	0	2	0	2	33.2	-4	-0.2	-12	-4	-2	0	-2	0	-7.3
10 52	88	86.1	17	4	1	1	1	1	33.6	95	90.1	23	2	0	1	1	1	18.2	7	4.0	6	-2	-1	0	0	0	-15.3
110	82	90.7	18	8	2	2	2	2	27.5	132	105.9	38	7	1	2	2	2	34.0	50	15.2	20	-1	-1	0	0	0	6.5
111	78	93.7	10	4	2	0	2	0	24.1	111	94.1	24	6	2	1	2	1	14.1	33	0.3	14	2	0	1	0	1	-10.0
123	88	80.5	24	4	1	1	1	1	21.0	83	78.6	18	8	2	2	2	2	22.4	-5	-2.0	-6	4	1	1	1	1	1.4
134	46	90.1	6	2	0	1	0	1	37.8	80	95.4	21	10	3	2	3	2	31.7	34	5.2	15	8	3	1	3	1	-6.2
221	93	86.5	17	8	3	1	3	1	23.9	83	90.5	21	5	0	2	1	2	32.2	-10	4.0	4	-3	-3	1	-2	1	8.3
257	84	98.7	13	6	2	1	2	1	23.0	117	88.5	23	7	1	2	2	2	20.4	33	-10.2	10	1	-1	1	0	1	-2.5
432	58	86.4	10	6	2	1	2	1	35.8	110	100.4	28	5	0	2	1	2	13.4	52	14.0	18	-1	-2	1	-1	1	-22.3
522	100	75.5	39	10	3	2	3	2	25.8	103	91.8	28	5	1	1	2	1	20.9	3	16.3	-11	-5	-2	-1	-1	-1	-5.0
537	84	84.2	15	4	1	1	1	1	31.8	75	96.5	18	4	1	1	1	1	27.0	-9	12.3	3	0	0	0	0	0	-4.8
20 74	89	95.6	18	6	2	1	2	1	33.9	71	85.2	11	2	0	1	0	1	30.8	-18	-10.4	-7	-4	-2	0	-2	0	-3.1
441	94	92.4	25	4	1	1	1	1	18.9	75	78.7	18	6	0	2	2	2	28.5	-19	-13.7	-7	2	-1	1	1	1	9.6
443	77	102.5	16	4	0	2	0	2	27.0	139	104.6	29	8	2	2	2	2	20.0	62	2.0	13	4	2	0	2	0	-7.0
510	84	91.7	30	14	5	2	5	2	26.3	107	94.1	31	11	0	5	1	5	24.7	23	2.5	1	-3	-5	3	-4	3	-1.6
511	107	84.0	24	6	2	1	2	1	27.7	104	85.1	24	4	0	1	2	1	27.4	-3	1.1	0	-2	-2	0	0	0	-0.2
533	104	90.1	10	4	0	2	0	2	26.4	83	93.5	22	6	0	2	2	2	28.9	-21	3.4	12	2	0	0	2	0	2.6
860	96	83.5	7	4	1	1	1	1	34.4	69	91.2	27	7	1	2	2	2	27.3	-27	7.7	20	3	0	1	1	1	-7.1
Average	84.70	88.97	17.30	5.90	1.60	1.35	1.60	1.35	28.28	94.05	91.84	22.05	5.65	0.70	1.75	1.50	1.75	24.95	9.35	2.87	4.75	-0.42	-0.95	0.37	-0.16	0.37	-3.33
SD	14.63	6.33	8.25	2.71	1.23	0.67	1.23	0.67	5.98	20.50	7.05	7.10	2.48	0.92	0.91	0.83	0.91	6.10	26.51	8.10	10.20	3.42	1.81	1.01	1.64	1.01	7.55

Table 6.4: Properties of 1 keV Cascades for a) Mg^{2+} and b) O^{2-} primary knock-ons.

a)

	Pure									Doped									Difference								
Direction	Peak No Frenkel Pairs (P_F)	Peak Time (fs) (P_T)	Displaced Atoms (N_T)	Total Defects (N_d)	Total Mg_i	Total O_i	Total V_{Mg}	Total V_O	Max dist between defects (Å)	Peak No Frenkel Pairs (P_F)	Peak Time (P_T) (fs)	Displaced Atoms (N_T)	Total Defects (N_d)	Total Mg_i	Total O_i	Total V_{Mg}	Total V_O	Max dist between defects (Å)	Peak No Frenkel Pairs (P_F)	Peak Time (fs) (P_T)	Displaced Atoms (N_T)	Total Defects (N_d)	Total Mg_i	Total O_i	Total V_{Mg}	Total V_O	Max dist between defects (Å)
021	175	109.6	46	12	3	3	3	3	50.5	179	90.5	42	12	3	3	3	3	46.5	4	-19.2	-4	0	0	0	0	0	-4.1
100	160	102.1	38	12	3	3	3	3	43.6	176	95.2	41	10	2	2	4	2	46.9	16	-6.9	3	-2	-1	-1	1	-1	3.3
10 31	158	100.5	38	14	5	2	5	2	47.3	118	102.3	67	13	3	3	4	3	62.1	-40	1.9	29	-1	-2	1	-1	1	14.8
10 52	188	103.7	49	12	3	3	3	3	35.2	161	92.0	39	11	1	3	4	3	39.6	-27	-11.7	-10	-1	-2	0	1	0	4.4
110	206	111.0	49	6	2	1	2	1	24.5	163	87.2	56	18	3	5	5	5	37.7	-43	-23.8	7	12	1	4	3	4	13.2
111	184	122.1	44	14	4	3	4	3	57.5	248	107.7	60	12	3	2	5	2	26.9	64	-14.4	16	-2	-1	-1	1	-1	-30.6
123	173	96.8	32	12	3	3	3	3	39.0	184	92.3	41	11	2	2	5	2	35.6	11	-4.6	9	-1	-1	-1	2	-1	-3.5
134	151	102.0	34	8	4	0	4	0	45.8	317	143.3	84	13	2	4	3	4	27.5	166	41.3	50	5	-2	4	-1	4	-18.3
221	144	103.1	25	10	3	2	3	2	43.6	149	114.7	62	8	2	2	2	2	58.4	5	11.6	37	-2	-1	0	-1	0	14.7
257	156	83.5	39	8	3	1	3	1	42.1	196	108.9	45	5	1	1	2	1	44.9	40	25.4	6	-3	-2	0	-1	0	2.7
432	155	116.4	54	16	4	4	4	4	59.7	166	120.1	47	11	3	2	4	2	57.8	11	3.7	-7	-5	-1	-2	0	-2	-1.9
522	158	87.8	32	8	3	1	3	1	38.2	202	114.2	38	7	1	1	4	1	39.6	44	26.5	6	-1	-2	0	1	0	1.4
537	143	99.2	39	12	4	2	4	2	41.3	197	101.3	45	12	3	2	5	2	43.7	54	2.0	6	0	-1	0	1	0	2.4
20 74	91	103.6	20	6	2	1	2	1	34.4	100	90.4	21	6	1	1	3	1	25.9	9	-13.2	1	0	-1	0	1	0	-8.5
441	58	105.2	17	10	4	1	4	1	34.5	149	113.7	42	8	2	1	4	1	62.6	91	8.5	25	-2	-2	0	0	0	28.1
443	99	91.1	16	6	1	2	1	2	32.7	127	114.2	21	5	1	1	2	1	16.9	28	23.1	5	-1	0	-1	1	-1	-15.9
510	82	88.2	17	6	2	1	2	1	31.8	81	85.5	25	7	1	2	2	2	25.7	-1	-2.6	8	1	-1	1	0	1	-6.1
511	73	99.7	18	4	1	1	1	1	32.8	110	100.9	17	5	1	1	2	1	29.0	37	1.2	-1	1	0	0	1	0	-3.8
533	96	93.4	25	6	2	1	2	1	21.5	103	102.9	27	9	1	3	2	3	21.4	7	9.4	2	3	-1	2	0	2	-0.1
860	122	98.2	26	10	3	2	3	2	23.3	110	91.4	15	8	2	2	2	2	24.7	-12	-6.9	-11	-2	-1	0	-1	0	1.4
Average	138.60	100.86	32.90	9.60	2.95	1.85	2.95	1.85	38.97	161.80	103.43	41.75	9.55	1.90	2.15	3.35	2.15	38.67	23.20	2.57	8.85	-0.05	-1.05	0.30	0.40	0.30	-0.30
SD	41.97	9.53	12.01	3.35	1.05	1.04	1.05	1.04	10.33	55.81	14.11	17.96	3.36	0.85	1.09	1.18	1.09	14.02	47.44	16.77	15.65	3.55	0.83	1.53	1.10	1.53	12.82

b)

	Pure									Doped									Difference								
Direction	Peak No Frenkel Pairs (P_F)	Peak Time (fs) (P_T)	Displaced Atoms (N_T)	Total Defects (N_d)	Total Mg_i	Total O_i	Total V_{Mg}	Total V_O	Max dist between defects (Å)	Peak No Frenkel Pairs (P_F)	Peak Time (fs) (P_T)	Displaced Atoms (N_T)	Total Defects (N_d)	Total Mg_i	Total O_i	Total V_{Mg}	Total V_O	Max dist between defects (Å)	Peak No Frenkel Pairs (P_F)	Peak Time (fs) (P_T)	Displaced Atoms (N_T)	Total Defects (N_d)	Total Mgi	Total Oi	Total VMg	Total VO	Max dist between defects (Å)
021	200	105.3	40	10	3	2	3	2	33.0	175	101.2	33	9	1	2	4	2	46.8	-25	-4.2	-7	-1	-2	0	1	0	13.8
100	181	97.4	30	8	2	2	2	2	36.9	170	89.6	44	15	3	3	6	3	37.7	-11	-7.8	14	7	1	1	4	1	0.8
10 31	159	116.7	49	12	3	3	3	3	39.7	122	97.2	33	15	3	3	6	3	65.0	-37	-19.5	-16	3	0	0	3	0	25.3
10 52	170	92.5	42	10	3	2	3	2	49.0	157	98.7	33	9	1	2	4	2	56.5	-13	6.2	-9	-1	-2	0	1	0	7.5
110	182	97.3	47	10	4	1	4	1	40.7	139	112.4	26	12	4	1	6	1	60.2	-43	15.1	-21	2	0	0	2	0	19.6
111	169	85.1	46	8	2	2	2	2	53.2	139	115.6	37	7	0	2	3	2	50.1	-30	30.5	-9	-1	-2	0	1	0	-3.2
123	188	97.7	46	12	2	4	2	4	37.0	187	117.3	48	10	2	3	2	3	48.1	-1	19.5	2	-2	0	-1	0	-1	11.1
134	167	91.2	27	6	1	2	1	2	35.3	125	102.3	21	8	3	1	3	1	57.2	-42	11.1	-6	2	2	-1	2	-1	21.9
221	224	105.4	35	8	1	3	1	3	53.0	168	115.5	51	13	2	3	5	3	63.7	-56	10.1	16	5	1	0	4	0	10.6
257	135	95.7	35	10	2	3	2	3	58.6	156	102.4	38	11	3	1	6	1	60.0	21	6.6	3	1	1	-2	4	-2	1.4
432	143	105.5	22	8	2	2	2	2	60.3	167	103.3	71	19	4	5	5	5	46.6	24	-2.2	49	11	2	3	3	3	-13.7
522	127	107.6	25	8	2	2	2	2	60.3	172	94.0	45	13	1	4	4	4	57.2	45	-13.6	20	5	-1	2	2	2	-3.1
537	126	110.2	29	6	1	2	1	2	56.2	155	100.0	42	13	3	3	4	3	53.2	29	-10.2	13	7	2	1	3	1	-3.0
20 74	89	95.6	18	6	1	2	1	2	33.9	71	85.2	11	2	0	1	0	1	30.8	-18	-10.4	-7	-4	-1	-1	-1	-1	-3.1
441	94	92.4	25	4	1	1	1	1	18.9	75	78.7	18	6	0	2	2	2	28.5	-19	-13.7	-7	2	-1	1	1	1	9.6
443	77	102.5	18	6	1	2	1	2	28.0	139	104.6	29	7	1	2	2	2	20.0	62	2.0	11	1	0	0	1	0	-8.0
510	84	91.7	30	14	5	2	5	2	26.3	107	94.1	30	11	0	5	1	5	24.7	23	2.5	0	-3	-5	3	-4	3	-1.6
511	107	84.0	24	6	2	1	2	1	27.7	211	110.8	33	4	0	2	0	2	37.2	104	26.7	9	-2	-2	1	-2	1	9.5
533	104	90.1	10	4	0	2	0	2	26.4	160	104.4	39	11	3	2	4	2	48.6	56	14.3	29	7	3	0	4	0	22.2
860	96	83.5	7	4	1	1	1	1	34.4	140	107.8	15	9	1	3	2	3	53.6	44	24.4	8	5	0	2	1	2	19.2
Average	141.10	97.38	30.25	8.00	1.95	2.05	1.95	2.05	40.44	146.75	101.75	34.85	10.20	1.75	2.50	3.45	2.50	47.28	5.65	4.37	4.60	2.05	-0.21	0.37	1.53	0.37	6.85
SD	43.38	9.07	12.21	2.83	1.19	0.76	1.19	0.76	12.83	34.64	10.20	13.76	4.01	1.41	1.19	1.93	1.19	13.28	42.38	14.58	16.48	4.06	1.93	1.30	2.17	1.30	11.22

Table 6.5: Properties of 2 keV Cascades for a) Mg^{2+} and b) O^{2-} primary knock-ons.

small. It is therefore not surprising that the average difference values are small compared to average property values. In other words, the overall effect on the lattice is not very great. However, this hides the significant effect that dopants have on properties predicted for a specific cascade generated by a PKA in a specific direction. In specific cases, the influence can be enormous, (though not always so). This is because, at this level of dopant (randomly distributed through the lattice), some cascades encounter more defects than others. Unfortunately, it has only been been possible to carry out one cascade simulation per direction for each PKA and energy combination. Presumably with higher PKA energies (and thus larger cascades), the number of defects encountered by cascades originating from different PKA directions is more similar.

What the study has shown is that the effect on N_d (and perhaps E_d) due to PKA orientation, predicted from perfect lattice simulations, is not a true reflection of reality. It is suggested here that the orientation anisotropy of N_d (and E_d) for a real material (i.e. one that incorporates a population of defects) should be rather less than for a hypothetical perfect lattice. This is because the change in property values due to having dopants in the lattice is small and while the individual differences can be large, they are not systematic. As such it should be expected that a different random distribution of defects should have a different effect on individual cascades. Exactly what the real orientation dependence for the present doped MgO lattice might be is yet to be derived since it requires sufficient results for each PKA to average over calculations repeated with different random dopant distributions.

Above, a rather general effect has been discussed, which conceivably might be caused by any suitable type of (scattering) defect population. A specific effect due to the charge compensating magnesium vacancies (V''_{Mg}) is now considered. To this end, it is necessary to compare the average values for N_d between a pure and doped lattice for a specific PKA species and energy. The values are fairly similar. However, the contributions to the average N_d values due to magnesium interstitial ions (Mg_i) are systematically smaller in the doped lattice than in the corresponding pure material. This is because ions generated during the cascade are being annihilated by pre-existing lattice V''_{Mg} defects (and thus do not count as defects). Examples are shown in figure 6.5. Consequently, the number of $Mg_i^{\bullet\bullet}$ ions is less than V''_{Mg} in the doped lattice (but these populations are, of course, equal in the pure material). (In an equilibrium situation this would be interpreted as a manifestation of the cation Frenkel equilibrium. Perhaps the initial stages of such a process are being seen here). Interestingly this reduction in $Mg_i^{\bullet\bullet}$ defects is being balanced by an increase in both O''_i and $V_O^{\bullet\bullet}$ defects (this is how N_d remains constant).

There are a number of other systematic changes that deserve comment. For all four combinations of PKA and energy, it is predicted that, in the doped lattice, there is a greater peak number of Frenkel pairs (P_F) and longer peak time (P_t). This subsequently translates into a greater number of displaced atoms (N_T). Conversely the nominal "size" of the cluster (maximum distance between defects) does not increase systematically. Caution should be taken when drawing conclusions from these data, however, since as previously mentioned, variations between specific directions are much greater than the

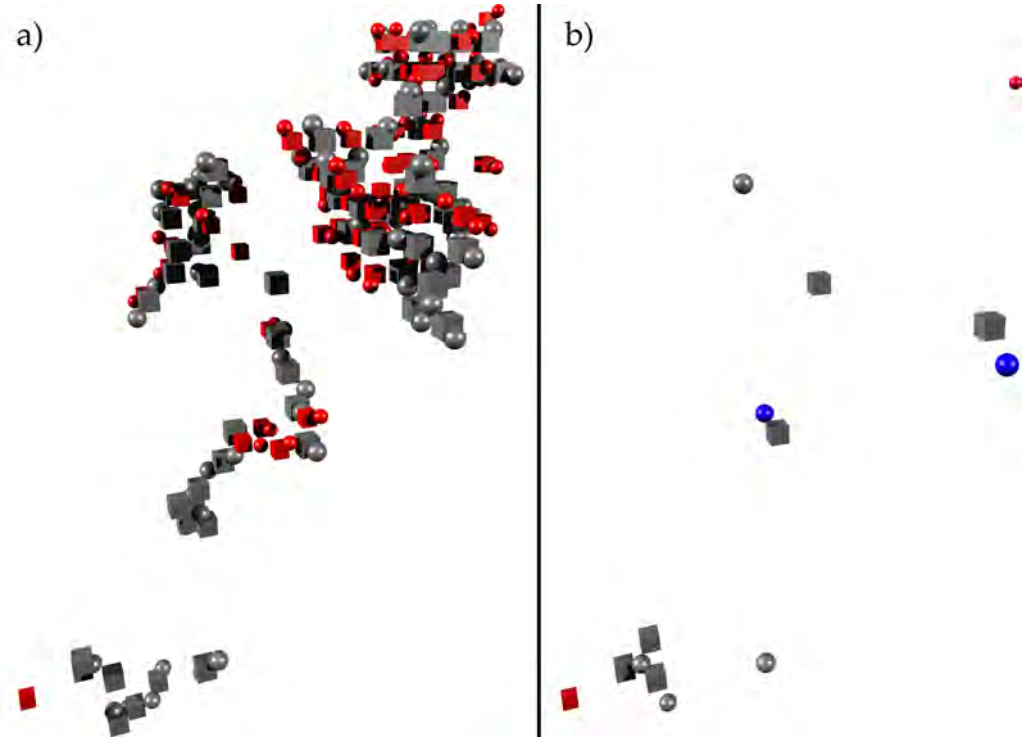

Figure 6.5: Damage induced by a 2 keV O^{2-} PKA in an alumina doped MgO lattice at a) peak damage (0.85 ps) and b) once the thermal-spike has dissipated (6 ps). Red indicates oxygen defects, grey magnesium defects; spheres are interstitial ions, cubes are vacancies. The blue spheres are magnesium ions that now occupy previously vacancy cation sites. Al impurities are not show in this figure.

change in average values. Nevertheless, that data would be commensurate with the view that, overall, the effect of the dopants is to slightly increase the disruption to the lattice but that does not translate to an increase in number of residual defects, N_d, once the thermal-spike has dissipated.

6.4.2 Examination of Some of the final Defect Clusters

Before some of the more common defect clusters are described, the nomenclature will be explained. In the following pages, intrinsic defects refer to those intrinsic to the MgO system and include $Mg_i^{\bullet\bullet}$, O_i'', V_{Mg}'' and $V_O^{\bullet\bullet}$; extrinsic damage is classified as those defects due to impurities, in this case $Mg_{Al}^{\bullet}$ and the charge compensating V_{Mg}'' defects above the intrinsic concentrations; and finally the radiation damage which can include defects of all kinds. This means that it is possible for defects caused by the radiation damage to anneal out the pre-existing damage due to the impurities.

In the doped case, many of the defects generated in the cascades at the 1 and 2 keV PKA energies studied, consist of isolated defects and small clusters of two or sometimes three interstitials. There is a strong tendency in the doped case for a magnesium interstitial ion produced from the cascade to migrate onto one of the extrinsic vacancies. An example of this is shown in figure 6.6a which shows an example from a 2 keV <110> Mg^{2+} PKA cascade. Figure 6.6b shows another common defect found in a different region of the same cascade. While this again shows the ability of the extrinsic vacancy to attract magnesium interstitials, it also shows the propensity of the $Al_{Mg}^{\bullet}$ substitutional defects to attract and trap oxygen interstitials. This configuration also forms when a magnesium-oxygen interstitial dimer migrates close to the $2Al_{Mg}^{\bullet}$:V_{Mg}'' system. It is also possible for an oxygen ion to be trapped by the $Al_{Mg}^{\bullet}$ defect without the Mg ion residing on the extrinsic vacancy as shown in figure 6.7.

Occasionally trimer interstitial groupings are formed (as observed in previous

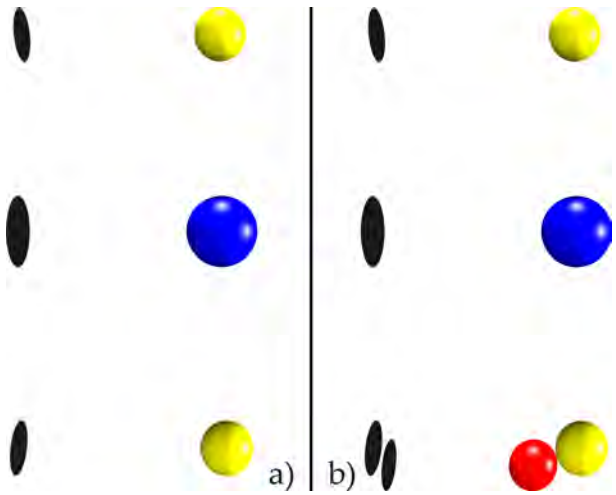

Figure 6.6: Simple defects found in 2% Al doped MgO. a) Radiation damage induced Mg interstitial captured by an extrinsic vacancy b) Same as a) but with a trapped O interstitial. Yellow sphere = $Al^{\bullet}_{Mg}$, blue sphere = $Mg^{\times}_{Mg}$, red sphere = O''_i.

Figure 6.7: O''_i trapped by $Mg^{\bullet}_{Al}$. Yellow = $Mg^{\bullet}_{Al}$. grey = V''_{Mg}. red = O''_i.

work [299]) in linear <100> combinations. Figure 6.8 shows an example $O''_i Mg^{\bullet\bullet}_i O''_i$ trimer that was formed as a consequence of the <134> 2 keV Mg^{2+} PKA simulation. These have been found to form in both pure and doped systems but are so infrequent that it is not possible to say if doping has any affect on the frequency of their occurrence. They seem to be less stable than the Mg-O interstitial dimer defect clusters in that (in this case) the oxygen defects tend to hop around the central Mg defect. On one occasion a defect of this type was seen to recombine with nearby vacancies by migrating

Figure 6.8: $O_i''Mg_i^{\bullet\bullet}O_i''$ trimer. Grey sphere = $Mg_i^{\bullet\bullet}$, red sphere = O_i''.

one hop along a <111> direction and then dissociating into a dimer and an oxygen interstitial.

Another relatively common defect is shown in figure 6.9. This is classified as a split di-vacancy and tends to form whenever there are 2 vacancies in a <111> configuration. If this occurs, the ion that forms the final corner of the three lattice sites migrates to the central interstitial site. Figure 6.9 shows the Mg version of this defect with an extrinsic V_{Mg}'' as one of the vacancies in the cluster. This has been shown to be more common than the O variant in the doped case due to the extrinsic Mg vacancies. In the pure case there seems to be no preference.

Due to the fact that vacancies are significantly less mobile than interstitials, it is far more common to see larger clusters of vacancies than interstitials as once a vacancy cluster forms, it is much less likely to move. It is also possible for uncommon configurations to remain to the end of the simulation. Figure 6.10 provides examples of two different configurations of vacancy trimers, a) shows a $V_{Mg}''V_O^{\bullet\bullet}V_{Mg}''$ right angle configuration from the 2 keV <573> O^{2-} PKA in doped MgO and b) shows a linear $V_O^{\bullet\bullet}V_{Mg}''V_O^{\bullet\bullet}$ cluster from the 2 keV

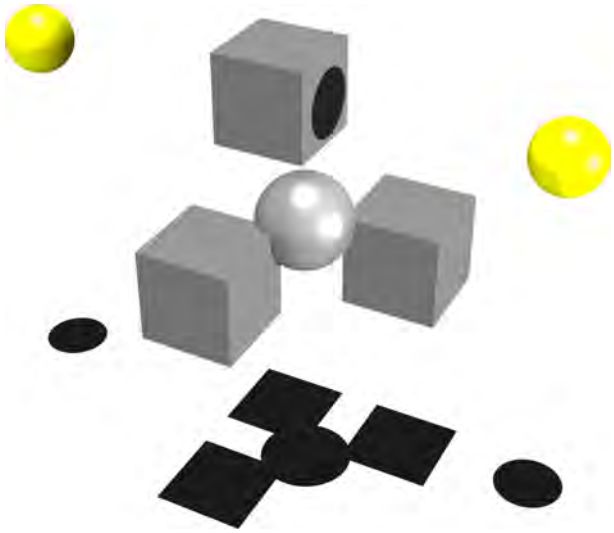

Figure 6.9: Split di-vacancy utilising an extrinsic V''_{Mg}. Grey cube = V''_{Mg} grey sphere = $Mg_i^{\bullet\bullet}$, yellow sphere = $Mg_{Al}^{\bullet}$.

<510>O^{2-} PKA in pure MgO.

This concludes the summary of defect clusters that were seen more than once. In isolated cascades there were highly complex defect configurations involving larger numbers of interstitials and vacancies but these were observed only once and are therefore not representative of the cascades as a whole. It is likely that the most important set of defects considered here were those pertaining to the capture of magnesium interstitial ions and the trapping of oxygen interstitials at the aluminium impurities as this is likely to have significant impact on recovery processes.

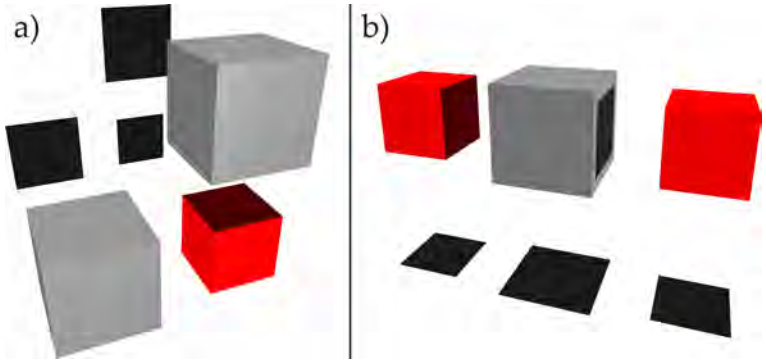

Figure 6.10: Vacancy trimer configurations. Grey cube = V''_{Mg}. Red cube = $V^{\bullet\bullet}_{O}$.

6.5 Conclusions

In their seminal paper Kinchin and Pease reported a model through which it is possible to estimate the maximum number of atoms permanently displaced from their lattice sites per PKA. Amongst the approximations in their model they neglected the anisotropy of E_d associated with the PKA incident direction and hence also the anisotropy in N_d. A number of computer simulation studies have focused on this issue, all of which assumed initially perfect lattice structures. It has been shown that the assumption of a perfect lattice is dubious because the variation in the predicted properties of a cascade, depends upon the local distribution of defects as much as it does on the PKA direction. Consequently, It is suggested that the anisotropy assumed from perfect lattice simulations is flawed and that any anisotropy should be much reduced as a result of the presence of lattice defects. Fifty years on it seems that at least one of the assumptions made by Kinchin and Pease may have been closer to the truth than has more recently been suggested.

Aside from the anisotropy issue it is difficult to quantify any substantial and systematic effect that the defects have on the evolution of the cascades due to insufficient results. It is possible, however, to postulate that recovery processes predicted by examining pure lattices are likely to be significantly modified. This can be justified by the analysis of the final defect population, mainly the trapping of oxygen interstitials adjacent to the Al substitutional defects and the similar effect the extrinsic vacancies have on the magnesium interstitials. It appears that such binding effects are significant although further work will be required to analyse this properly; see chapter 7 for more information.